Available online at www.sciencedirect.com
SCIENCE DIRECT®
Deep-Sea Research I 51 (2004) 2073–2090
DEEP-SEA RESEARCH PART I
www.elsevier.com/locate/dsr

Does the Ulleung eddy owe its existence to β and nonlinearities?

Wilton Z. Arruda[a], Doron Nof[b,*], James J. O'Brien[c]

[a]Departamento de Métodos Matemáticos, Universidade Federal do Rio de Janeiro, Brazil
[b]Department of Oceanography 4320 and Geophysical Fluid Dynamics Institute, Tallahassee, FL 32306-4320, USA
[c]Center for Ocean-Atmospheric Prediction Studies, The Florida State University, Tallahassee, FL 32306-2840, USA

Received 2 June 2003; received in revised form 17 December 2003; accepted 28 July 2004
Available online 7 October 2004

Abstract

A nonlinear theory for the generation of the Ulleung Warm Eddy (UWE) is proposed. Using the nonlinear reduced gravity (shallow water) equations, it is shown analytically that the eddy is established in order to balance the northward momentum flux (i.e., the flow force) exerted by the separating western boundary current (WBC). In this scenario, the presence of β produces a southward (eddy) force balancing the northward momentum flux imparted by the separating East Korean Warm Current (EKWC).

It is found that, for a high Rossby number EKWC (i.e., highly nonlinear current), the eddy radius is roughly $2R_d/\varepsilon^{1/6}$ (here $\varepsilon \equiv \beta R_d/f_0$, where R_d is the Rossby radius), implying that the UWE has a scale larger than that of most eddies (R_d). This solution suggests that, in contrast to the familiar idea attributing the formation of eddies to instabilities (i.e., the breakdown of a known steady solution), the UWE is an integral part of the steady stable solution. The solution also suggests that a weak WBC does not produce an eddy (due to the absence of nonlinearity).

A reduced gravity numerical model is used to further analyze the relationship between β, nonlinearity and the eddy formation. First, we show that a high Rossby number WBC which is forced to separate from the wall on an f plane does not produce an eddy near the separation. To balance the northward momentum force imparted by the nonlinear boundary current, the f plane system moves constantly offshore, producing a southward Coriolis force. We then show that, as β is introduced to the problem, an anticyclonic eddy is formed. The numerical balance of forces shows that, as suggested by the analytical reasoning, the southward force produced by the eddy balances the northward flow force imparted by the boundary current. We also found that the observed eddy scale in the Japan/East Sea agrees with the analytical estimate for a nonlinear current.

Keywords: Japan/East Sea; Ulleung Warm eddy; Intrusion eddy; East Korea Warm Current; Western Boundary Currents

*Corresponding author. Department of Oceanography 4320, Florida State University, Tallahassee, FL 32306-4320, USA. Tel.: +1-850-644-2736; fax: +1-850-644-2581.
E-mail address: nof@ocean.fsu.edu (D. Nof).

0967-0637/$ - see front matter © 2004 Elsevier Ltd. All rights reserved.
doi:10.1016/j.dsr.2004.07.014

Nomenclature

f	Coriolis parameter ($f_0 + \beta y$)
g'	reduced gravity, $g\,\Delta\rho/\rho$
h	upper layer thickness
h_e	Eddy upper layer thickness
H	undisturbed upper layer thickness
H_e	upper layer thickness at the eddy center
L	boundary current width (Figs. 4 and 10)
L_2	width of square domain S (Fig. 4)
L_e	basin zonal width (3)
R	Eddy radius
R_1	parameter defined as $8(g'H_e)^{1/2}/f_0$
R_d	Rossby radius of deformation, $(g'H_e)^{1/2}/f_0$
R_{de}	Rossby deformation radius of the eddy, $(g'H_e)^{1/2}/f_0$
S	integration area bounded by ABCD in Figs. 4 and 10
S^+ ,S^-	subsets of S such that $y > y_0$ and $y \leqslant y_0$ respectively (Fig. 4)
u, v	velocity components in Cartesian coordinates
$\bar{v}$	current's mean speed
v_θ	orbital velocity in the eddy
y_s, y_n	y-coordinates of southern and northern boundaries of S respectively (Figs. 4 and 10)
x_B	x-coordinate of point B in Fig. 10
β	variation of the Coriolis parameter with latitude
ε	small parameter equal to $\beta R_d/f_0$
$\rho, \Delta\rho$	Density and density difference between the layers
ν	viscosity coefficient
κ	coefficient of interfacial friction
ψ	streamfunction (defined by $\psi_y = -uh; \psi_x = vh$)
ψ_∞	limit of ψ as $x \to \infty$
ψ_e	Eddy streamfunction
τ^x	zonal component of the wind stress
ADCP	Acoustic Doppler Current Profiler
EKWC	East Korean Warm Current
JES	Japan/East Sea
NKCC	North Korea Cold Current
TWC	Tsushima Warm Current
UWE	Ulleung Warm Eddy
WBC	Western Boundary Current

1. Introduction

The Japan/East Sea (JES) is in many respects analogous to the much more frequently studied Mediterranean Sea as both are marginal seas with convection regions and strong eddies. The main difference between the two is that the JES has more than one connection to its adjacent ocean and, in view of this, it is flushed by wind-driven flows which enter through one gap and exit through the others. For a review of the JES, the reader is referred to Preller and Hogan (1998). Our main focus here is to provide an explanation for the generation of the Ulleung Warm Eddy (UWE).

1.1. Observational background

The northward-flowing Tsushima Warm Current (TWC) has a major impact on the circulation of the JES (Preller and Hogan, 1998). Perkins et al. (2000) and Jacobs et al. (2001) verified the earlier ideas that, within the Tsushima Strait, the TWC is divided into two different currents, one flowing through the eastern channel and the other through the western channel. This so-called "primary branching"(Fig. 1) is thought to be due to the Tsushima Island and the topography, but Ou (2001) proposed an alternative splitting mechanism. According to the classical interpretation of Suda and Hidaka (1932) and Uda (1934), the northern part of the TWC ultimately splits again, forming a total of three distinct branches (Fig. 1) originally named (from east to west) the first, second and third branches. The structure and variability of the TWC were studied using a variety of data sets: hydrographic (Kawabe, 1982a; Lie, 1984; Lie and Byun, 1985; Kim and Kim, 1983; Katoh, 1994; Preller and Hogan, 1998), satellite-derived sea-surface temperature (SST) (Kim and Legeckis, 1986; Cho and Kim, 1996), and numerical model experiments (Kawabe, 1982b; Hogan and Hurlburt, 2000).

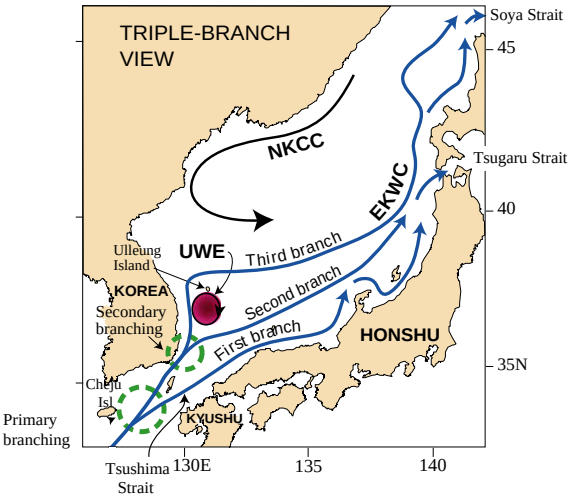

Fig. 1. Schematic diagram of the TWC and the triple branch view (in blue) with the first branch, second branch, and third branch (sometimes referred to as the EKWC). The broken green circles show the splitting of the TWC and the closed red circle represents the UWE. The NKCC opposes the EKWC (adapted from Preller and Hogan, 1998).

For clarity, we shall refer to the East Korean Warm Current (EKWC) as the "third branch" of the TWC. As shown in Fig. 1, this branch separates from the coast at 37–38°N. This separation appears to be analogous to the classical WBC separation that occurs around 37–38°N, but, as will be shown later, it is probably forced by the Tsugaru Strait outflow (situated to the east) which induces a net upstream northward flow within the JES. This is because the JES is simply too narrow, compared to the Atlantic and the Pacific, to allow for a wind-induced separation.

Using acoustic doppler current profiler (ADCP) data, Katoh (1994) estimated that the transport of the EKWC mounted to about 1.54 Sv in June 1988, 0.70 Sv in August 1988, and 1.77 Sv in June 1989. In general, the current is strong in the spring and summer and weak in the winter. We shall later argue that, because the generation of the UWE requires nonlinearity (i.e., strong current), our proposed mechanism allows the establishment of the eddy only during the spring and summer, in agreement with the observations. Tanioka (1968) argued that 80–90% of the volume transport of the EKWC returns southward around Ulleung Island forming the UWE (see also Ichiye and Takano, 1988; Kang and Kang, 1990; Kim et al., 1991; Katoh, 1994; Mitchell, 2003). The UWE is located in the central part of the Ulleung Basin (where the depth exceeds 1500 m) and has a diameter of approximately 150 km (Fig. 2).

Isoda and Saitoh (1993) reported the formation of a northward flow near the Korean coast when the eddy approaches the western slope of the continental margin; however, the eddy does not always migrate. Lim and Kim (1995) argued that topography is controlling the eddy's position. Using satellite-tracked drifters, Lie et al. (1995) showed that the eddy was almost stationary from December 1992 to September 1993. They also suggested that the EKWC splits further into two parts—the main stream, which meanders around Ulleung Island, and a branch flowing northeast along the Korean coast. Besides the UWE, the JES shows high eddy activity and various studies examined the horizontal eddy scales in the basin

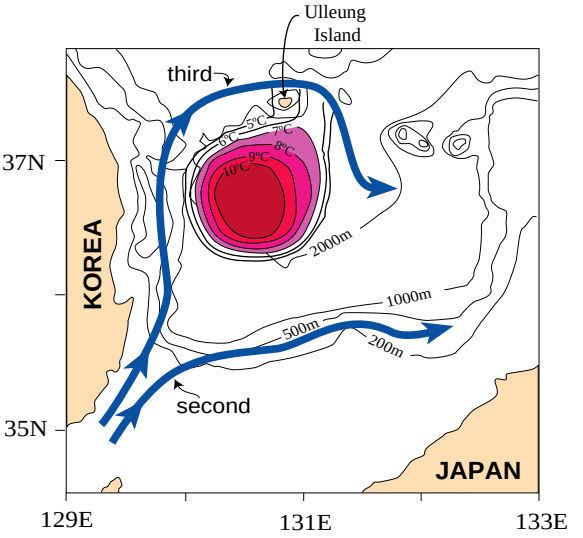

Fig. 2. Bathymetry and horizontal temperature distribution at 200 m depth during July 8–15, 1989, showing the UWE. The temperature contour interval is 1 °C. The blue arrowed lines show the third branch (EKWC) and the second branch (adapted from Katoh, 1994 and Lim and Kim, 1995). Note that at times the eddy is situated farther to the North (Katoh, 1994).

(Toba et al., 1982; Kim and Legeckis, 1986; Seung and Kim, 1989; Ichiye and Takano, 1988; Tameishi, 1987; Matsuyama et al., 1990; Isoda and Nishihara, 1992; Sugimoto and Tameishi, 1992; Miyao, 1994; Holloway et al., 1995; Yoon and Kawamura, 2002). Recently, Gordon et al. (2002) and Ou and Gordon (2002) addressed the issue of intrathermocline (subsurface) eddies in the JES. Although these studies are of interest, they are probably not related to the UWE which has a strong surface signature.

1.2. The EKWC separation

As mentioned, our aim is to provide an explanation for the establishment of the UWE. To do so, we shall consider an EKWC separation forced by the net northward throughflow induced by the Tsugaru outflow to the east. Even though the Tsugaru Strait is situated at 41.5°N and the EKWC separates slightly to the south at 37–38°N, we see no mechanism explaining the separation other than the Tsugaru outflow and its associated (upstream) northward flow within the basin. As will be shown below, this throughflow-induced separation is different from the classical wind-induced WBC separation discussed in earlier articles (e.g., Parsons, 1969; Veronis, 1973; Huang and Flierl, 1987; Dengg et al., 1996). It is also different from the collision-induced separation suggested by Lebedev and Nof (1996, 1997).

We shall first examine the issue of whether the momentum flux of the opposing North Korea Cold Current (NKCC) is negligible. Second, we shall show that the outflow through the Tsugaru Strait in the eastern JES is most likely the cause of the separation because it forces a northward flow within the basin, implying a thick upper layer along the eastern boundary and a thin upper layer along the western boundary. As this throughflow proceeds northward, the thickness along the western boundary gradually decreases (due to β) and ultimately vanishes. We will then argue that the fact that the EKWC separates somewhat to the south of the Tsugaru Strait is due to the NKCC which pushes it southward away from the location where it would have separated without it.

1.2.1. The EKWC and NKCC momentum fluxes

We shall now show that, when the EKWC is strong (spring and summer), the NKCC momentum flux is relatively small compared to the momentum flux of the EKWC. To see this, we note that the momentum flux of each boundary current can be approximated as

$$\int_0^\infty hv^2\,\mathrm{d}x \simeq \bar{v}\int_0^\infty hv\,\mathrm{d}x, \tag{1}$$

where $\bar{v}$ and $\int_0^\infty hv\,\mathrm{d}x$ are the average speed and the transport over the boundary current, respectively. Observations (Gordon, 1990; Preller and Hogan, 1998; Rostov et al., 2001) suggest that the strong EKWC has a transport of $\sim$1.5 Sv and a speed of $\sim$25 cm s^{-1}, while the NKCC has a transport of $\sim$0.5 Sv and a speed $\sim$5 cm s^{-1}. This gives a momentum flux ratio of 1/15, indicating that the momentum flux of the NKCC is usually negligible.

Note, however, that these values change on various time scales and that, consequently, the momentum flux of the NKCC is not always negligible. Using ADCP data collected during June–July 1999, Ramp et al. (2003) computed a transport of 1.45 Sv and a momentum flux of $2.27\times10^5\,\mathrm{m^4\,s^{-2}}$ for the EKWC and a transport of 0.78 Sv and momentum flux of $1.59\times10^5\,\mathrm{m^4\,s^{-2}}$ for the NKCC. This gives a ratio of 0.7 for the momentum fluxes, which is clearly not negligible. It is important to realize that, for the time period considered by Ramp et al. (2003), no UWE was observed. Consequently, they were able to apply the theory for the collision of boundary currents on an f plane (Agra and Nof, 1993) and conclude that the separated current should leave the coast at a calculated angle of 80°, which was in very good agreement with their observations.

1.2.2. The EKWC separation process

To see that, for most of the year, the wind stress (which is the classical force associated with separation) does not play an important role in the EKWC separation, consider the depth-integrated linear reduced gravity x-momentum

equation,

$$-fV = -\frac{g'}{2}\frac{\partial(h^2)}{\partial x} + \frac{\tau^x}{\rho}, \quad (2)$$

where h is the upper layer thickness, V is the vertically integrated velocity component in the y direction, g' the reduced gravity, τ^x the zonal wind stress component (assumed to be a function of y only) and ρ is the upper layer density. Integrating (2) zonally across the basin and temporarily assuming that there is no net meridional volume transport through the section (i.e., no "sink" and no throughflow through the Tsugaru Strait), we have,

$$h_{eb}^2 - h_{wb}^2 = \frac{2\tau^x}{\rho g'} L_e,$$

where h_{wb} and h_{eb} are the (wind-induced) upper layer thicknesses on the western boundary and eastern boundary (respectively), and L_e is the basin length. Note that, since we merely want to show here that the wind alone cannot cause separation, we have temporarily (and temporarily only) neglected the outflow-induced meridional transport. At the separation latitude $h_{wb} = 0$, implying,

$$h_{eb} = \left(\frac{2\tau^x}{\rho g'} L_e\right)^{1/2}. \quad (3)$$

Using (3) and the climatological Hellerman–Rosenstein zonal wind stress for 37°N, we can calculate monthly values for the no-sink wind-induced upper layer thickness h_{eb}. From November to March, the average zonal wind stress is high ($0.078\,\mathrm{N\,m^{-2}}$ for January) which, together with $L_e \sim 1000$ km and $g' \sim 2\times10^{-2}\,\mathrm{m\,s^{-2}}$, gives a mean value of 57 m for h_{eb}. For the rest of the year, the average zonal wind stress is much weaker (giving an h_{eb} of 10 m for April) and even negative from May to October. According to Chu et al. (2001), the upper layer thickness on the eastern boundary is between 150 and 200 m from November to April, indicating that, even during the strong wind stress period, the calculated h_{eb} is too small to allow for a wind-induced separation. The difference between the wind setup thickness of 10–50 m to the actual thickness along the eastern boundary of 100–200 m is so large that even if the actual wind stress were double what we have taken, a wind-induced separation would still be impossible.

On this basis, we conclude that the JES has a too short zonal width (i.e., it is too narrow) to accommodate separation of the EKWC by the local wind stress, indicating that the Tsugaru Strait outflow (which induces a net northward mass flux in the basin) is the main mechanism responsible for the EKWC separation. To see this, we note (from the geostrophic transport formula, $T = g'h^2/2f$, with $g' \sim 2\times10^{-2}\,\mathrm{m\,s^{-2}}$ and $f \sim 10^{-4}\,\mathrm{s^{-1}}$) that a net meridional flow of merely 2 Sv (which leaves the basin through the Tsugaru Strait) is sufficient to create a thickness of 150 m along the eastern boundary and zero (separation causing) thickness along the western boundary. (Note that this flow is driven by the wind field over the Pacific and not in the JES (Nof, 2003).) By the same token, it is important to recognize that the Tsugaru Strait is probably not the only active mechanism, as otherwise the separation would have occurred at the same latitude as the Tsugaru Strait (41.5°N). As mentioned, the opposing NKCC is probably the agent responsible for pushing the EKWC slightly to the south, causing it to separate at 37–38°N rather than 41.5°N.

1.3. Objectives of the present study

Before addressing our objectives, it should be pointed out that other WBCs also produce eddies when they separate. Observations of the East Australian Current and numerical simulations of the Brazil Current (Olson, 1991) suggest that the separation mechanism of the WBC leads to the formation of an "intrusion eddy".[1] The reader is referred to Nilson and Cresswell (1980) and to Tomczak and Godfrey (1994) for a thorough discussion of the East Australian Current eddies (pp. 136–139) and to Tomczak and Godfrey (1994) for a description of the Brazil Current problem (pp. 270–272). In what follows, we shall argue that the UWE belongs to a similar category. The identification of physical mechanism responsible

[1]This term was first used by Olson (1991) to describe an eddy associated with a western boundary current separation.

for the existence of the intrusion eddy is the focus of this paper.

Our proposed eddy generation mechanism is shown in Fig. 3a. Upon separation, the WBC creates an imbalance in the longshore momentum flux (sometimes referred to as "flow force" or jet force) because, when it turns to the right, there is no obvious force which can balance its northward upstream force. A large "intrusion eddy" is established because, on a β plane, such an eddy produces a southward force which can balance this upstream WBC flow force. Such a balance is, of course, required if a steady state is to be reached. (On an f plane such a balance is not possible, so the system continuously evolves in time.) Note that by "steady state" we merely mean here that the WBC exists in its strong state (spring and summer) for a period longer than $O(\beta R_d)^{-1}$ (which is typically 10–14 days). This is certainly true for the EKWC. Although the physical situation is quite different, a similar balance of forces exists in the outflow from the Tsugaru Strait (Nof and Pichevin, 1999). In that case, the balance is responsible for the generation of the *Tsugaru* gyre.

This paper is organized as follows: In Section 2, we derive an analytical relationship that represents the balance of forces in a control region surrounding the eddy. We also derive an estimate for the eddy radius based on the relation found earlier. In Section 3, we describe the comparison between the analytical results from the previous sections and the outputs of numerical model. In Section 4 we investigate the linear limit and in Section 5 we discuss the results and present the conclusions.

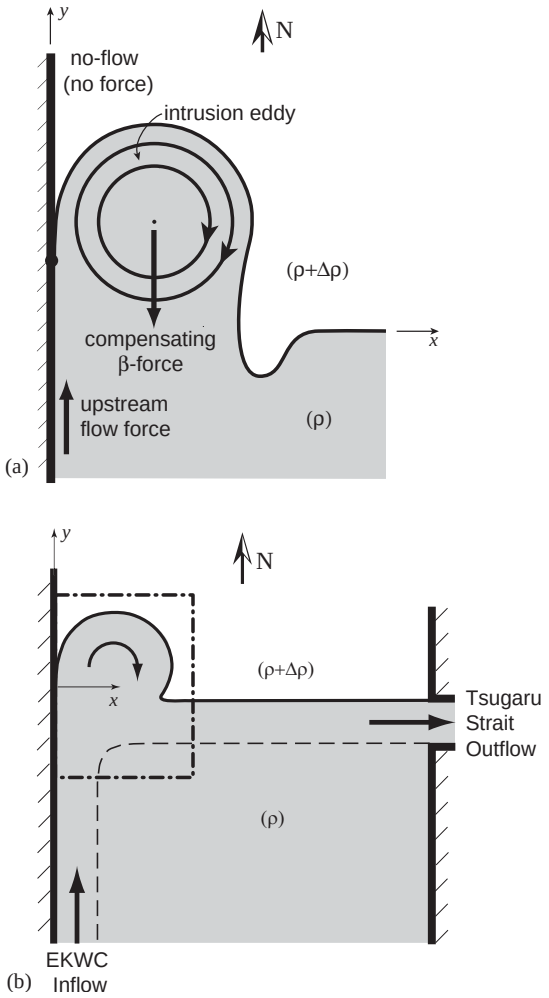

Fig. 3. (a) The nonlinear balance of flow forces associated with the WBC separation. A northward flow upstream generates a northward force similar to that associated with a jet exiting a rocket. Beyond the separation, there is no force to balance it. It is, therefore, balanced by a southward β force associated with the eddy which is established in order to offset the nonlinear upstream (WBC) force. The β force is generated because all particles circulating anticyclonically within the eddy sense a larger Coriolis force on the northern side than they do on the southern side. As a result, the southward Coriolis force in the northern part of the eddy is greater than the northward Coriolis force on the southward part of the eddy. Consequently, a net southward force is established. (A northward force is generated when cyclones are placed on a β plane.) In the linear limit there is no upstream force (because this force is proportional to the square of the meridional velocity) and, therefore, no eddy. (b) Schematic diagram of the separation of the EKWC forced by the Tsugaru outflow on the eastern side of the basin and the associated northward flow in the basin. The shaded area represents the region where the lighter layer is present. The origin of the coordinate system is situated at the separation point. A close-up of the region bounded by the dashed–dotted line is shown in Fig. 4. Note that, in reality, the separation of the EKWC from the western boundary occurs at 37–38°N, which is south of the Tsugaru Strait (42°N). We believe that this mismatch in latitudes is due to the NKCC which opposes the EKWC and forces it to separate south of where it would have separated without. There is also a mismatch between the actual separation of the EKWC from the boundary and the position of the actual front (39–40°N). This mismatch is neglected in our model.

2. Formulation

We shall study the "intrusion eddy" (formed when a WBC separates from the coast due to an outflow east of the boundary) in the framework of a baroclinic reduced gravity model on a β plane (Fig. 3b). Though the wind stress and the ocean interior are responsible for the existence of the WBC in the first place, we assume that their role in the dynamics of the eddy is minor, because the basin length scale of the wind systems is much greater than that of the boundary current [$\sim O(R_d)$].

Consider a single northward-flowing WBC in an upper layer (with density ρ) above an infinitely deep layer of slightly denser water (with density $\rho+\Delta\rho$). As the current flows northward, it reaches a latitude where the upper layer thickness vanishes on the wall due to the outflow to the east (which induces a net northward flow in the basin) and, consequently, separation takes place. We place the origin of our coordinate system right at the separation point (on the wall) and assume that, far away from the western boundary and far south from the separation latitude, the upper layer thickness approaches an undisturbed value H.

As alluded to earlier, the effects of an opposing southward-flowing boundary current are neglected.

The separated current forms a front where the outcropping streamline divides the domain into two sections. As we shall see later, it will not be necessary to derive the solution for the entire region and the latitude of the separation point because we shall use an integrated approach which avoids that need. A schematic diagram of our domain of study is depicted in Fig. 4.

2.1. North–South momentum balance

Assuming a steady state and integrating (after multiplying by h) the steady and inviscid nonlinear y-momentum equation,

$$u\frac{\partial v}{\partial x}+v\frac{\partial v}{\partial y}+fu+g'\frac{\partial h}{\partial y}=0,$$

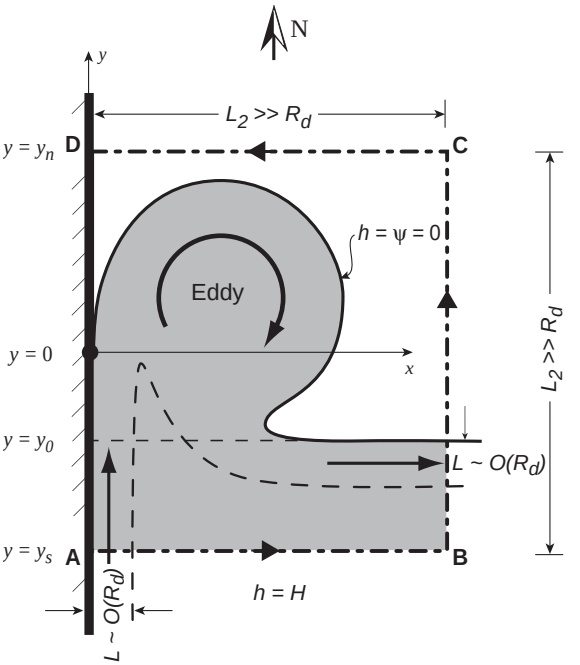

Fig. 4. A close-up of the region bounded by the dashed–dotted line in Fig. 3b. A northward-flowing western boundary current (WBC) (with width of $O(R_d)$) in a layer of density ρ separates from the coast and forms an intrusion eddy. After the fluid circles within the eddy, it flows zonally eastward. H is the undisturbed upper layer thickness at the basin interior. It is shown that the eddy scale is of $O(R_d/\varepsilon^{1/6})$ and that the momentum imparted on the region bounded by $ABCD$ (through AB) by the boundary current is balanced by the β-induced force of the anticyclonic eddy. S^+ and S^- are the shaded areas north and south of y_0, respectively.

over the fixed region S bounded by the dashed line $ABCDA$ shown in Fig. 4, we get,

$$\iint_S\left(hu\frac{\partial v}{\partial x}+hv\frac{\partial v}{\partial y}\right)\mathrm{d}x\,\mathrm{d}y+\iint_S(f_0+\beta y)uh\,\mathrm{d}x\,\mathrm{d}y+\frac{g'}{2}\iint_S\frac{\partial(h^2)}{\partial y}\,\mathrm{d}x\,\mathrm{d}y=0, \tag{4}$$

which, by using the continuity equation and streamfunction ψ, we obtain,

$$\iint_S\left[\frac{\partial(huv)}{\partial x}+\frac{\partial(hv^2)}{\partial y}\right]\mathrm{d}x\,\mathrm{d}y-\iint_S(f_0+\beta y)\frac{\partial\psi}{\partial y}\,\mathrm{d}x\,\mathrm{d}y+\frac{g'}{2}\iint_S\frac{\partial(h^2)}{\partial y}\,\mathrm{d}x\,\mathrm{d}y=0 \tag{5}$$

Here, the notation is conventional, i.e., u and v are the velocity components in the x and y directions, h is the upper layer thickness, ψ is the transport streamfunction defined by $\partial\psi/\partial y = -uh; \partial\psi/\partial x = vh$, and g' is the reduced gravity, $g\Delta\rho/\rho$ (for convenience, variables are defined in both the text and in the Nomenclature). Application of Green's theorem to (5) gives

$$\oint_{\partial S} huv\,\mathrm{d}y - \oint_{\partial S}\left(hv^2 + \frac{g'h^2}{2}\right)\mathrm{d}x + f_0\oint_{\partial S}\psi\,\mathrm{d}x + \beta\oint_{\partial S} y\psi\,\mathrm{d}x + \beta\iint_S \psi\,\mathrm{d}x\,\mathrm{d}y = 0, \tag{6}$$

where ∂S is the boundary of S.

Next, we assume that $\psi = 0$ along the wall and the outcropping front and note that at least one of the three variables h, u, and v vanishes on every portion of the boundary ∂S. It then follows from (6) that

$$\int_B^A \left[hv^2 + \frac{g'h^2}{2} - (f_0 + \beta y)\psi\right]\mathrm{d}x - \beta\iint_S \psi\,\mathrm{d}x\,\mathrm{d}y = 0, \tag{7}$$

Assuming now that both upstream and downstream the flow is geostrophic in the cross-current direction, we get (after multiplying the geostrophic relation $(f_0 + \beta y)v = g'\partial h/\partial x$ by h and integrating on the segment AB),

$$(f_0 + \beta y)\psi + C = \frac{g'}{2}h^2, \tag{8}$$

where C is a constant to be determined. Note that at $x \to \infty$ the flow is geostrophic in the y-direction so that,

$$(f_0 + \beta y)uh = \frac{-g'}{2}\frac{\partial(h^2)}{\partial y},$$

and integration in y gives,

$$(f_0 + \beta y)\psi\Big|_{y_s}^{y_n} - \beta\int_{y_s}^{y_n}\psi_\infty\,\mathrm{d}y = \frac{g'}{2}h^2\Big|_{y_s}^{y_n},\ x \to \infty,$$

where ψ_∞ (which is a function of y) is the streamfunction at $x \to \infty$, and y_s and y_n are the y components of points A and D (Fig. 4), respectively. Since $\psi = h = 0$ at $y = y_n$, it follows that $C = -\beta\int_{y_s}^{y_n}\psi_\infty\,\mathrm{d}y$ so that (7) can be written as

$$\int_0^L hv^2\,\mathrm{d}x - \beta\iint_S (\psi - \psi_\infty)\,\mathrm{d}x\,\mathrm{d}y = 0, \tag{9}$$

where L is the width of the boundary current. Note that the integrand of the second integral vanishes as $x \to \infty$ and, consequently, the integral does not change when the zonal extent of S is increased (as should be the case).

The first term in (9) is the (order one) northward momentum flux of the WBC. The second term corresponds to the difference between the flow induced by the separation and the flow downstream (ψ_∞). We immediately see that this anomaly must be positive (i.e., $\psi - \psi_\infty > 0$) and large because $\beta\ell/f$ (where ℓ is the region length scale) is small. A large anticyclone fits those two requirements. Relation (9) also shows that there cannot be a steady solution on an f plane ($\beta \equiv 0$) because there is no force to balance the upstream momentum flux (the first term). We shall see later (Section 3.2) that this implies an offshore migration (in the f plane case).

For simplicity, we rewrite (9) as

$$\int_0^L hv^2\,\mathrm{d}x - \beta\iint_{S^+}(\psi - \psi_\infty)\mathrm{d}x\,\mathrm{d}y - \beta\iint_{S^-}(\psi - \psi_\infty)\mathrm{d}x\,\mathrm{d}y = 0, \tag{10}$$

where S^+ and S^- are subsets of S corresponding to $y > y_0$ and $y \leqslant y_0$, respectively (see Fig. 4). We shall now leave (10) aside temporarily and discuss the relevant scales.

2.2. Scaling

Assuming nonlinear dynamics and the balance implied by (9), we take the following scales:

$$L \sim O(R_\mathrm{d}), v \sim O\left[(g'H)^{1/2}\right],$$

$$\psi \sim O\left(\frac{g'H^2}{f_0}\right) \quad \text{outside the eddy},$$

$$\psi \sim O\left(\frac{g'H_\mathrm{e}^2}{f_0}\right) \quad \text{inside the eddy},$$

where $R_\mathrm{d} = (g'H)^{1/2}/f_0$ is the Rossby deformation radius, and $H_\mathrm{e} \gg H$ is the depth scale for the

eddy. The large eddy scale (ψ and H_e) reflects the momentum balance which, as mentioned above, implies that ψ must be large and positive.

Note that the integrand of the third term in (10) is zero in the area outside the region influenced by the separation, so each of the three terms in (10) can be scaled as,

$$\int_0^L hv^2\,\mathrm{d}x \sim O\left(g'H^2R_\mathrm{d}\right), \tag{11}$$

$$\beta\iint_{S^+}\psi\,\mathrm{d}x\,\mathrm{d}y \sim O\left(\beta R_{\mathrm{de}}^2\frac{g'H_\mathrm{e}^2}{f_0}\right), \tag{12}$$

$$\beta\iint_{S^-}(\psi-\psi_\infty)\,\mathrm{d}x\,\mathrm{d}y \sim O\left(\beta R_\mathrm{d}L_2\frac{g'H^2}{f_0}\right), \tag{13}$$

where $R_{\mathrm{de}}=(g'H_\mathrm{e})^{1/2}/f_0$, and L_2, the length of the integration domain $ABCD$ (Fig. 4), is much larger than R_d. Note that the ratio between the third and first terms is $\beta L_2/f_0 \ll 1$. Consequently, only the second term can balance the first term. Taking accordingly,

$$R_{\mathrm{de}} \sim O\left(\frac{R_\mathrm{d}}{\varepsilon^{1/6}}\right) \tag{14}$$

and

$$L_2 \sim O(R_{\mathrm{de}}), \tag{15}$$

where $\varepsilon=\beta R_\mathrm{d}/f_0 \ll 1$, we now have a balance between the first and second terms. The ratio between the first term and the third term is $O(\varepsilon^{5/6})$.

Two comments should be made with regard to the above scales. First, as is frequently the case, the scaling may conceal potentially large numbers such as powers of the known $2\sqrt{2}$ ratio between the eddy radius and the Rossby radius (see, e.g., Nof, 1981; Killworth, 1983). Second, the 1/6 power of ε implies that, for most cases [$\varepsilon\sim$O (0.1)], R_{de} will be comparable to R_d (though it will be somewhat larger).

2.3. Solution

The scale analysis shows that the leading order nonlinear balance is

$$\int_0^L hv^2\,\mathrm{d}x = \beta\iint_{S^+}\psi\,\mathrm{d}x\,\mathrm{d}y. \tag{16}$$

As expected, this momentum constraint is not sufficient to close the problem and one needs to invoke other information such as the distribution of vorticity to obtain a solution. For simplicity, we shall first look at the case where both the eddy and the WBC have zero potential vorticity (pv) (i.e., the highly nonlinear case). Note that, for this zero-pv limit, the solutions for both the boundary current and the eddy are straightforward despite the nonlinearity. We shall see later that, with this limit, we obtain a lower bound on the eddy radius.

2.3.1. Zero-pv boundary current

For a zero-pv northward-flowing boundary current,

$$v=\begin{cases} f(L-x), & x\leqslant L,\\ 0, & x>L,\end{cases} \tag{17}$$

$$h=\begin{cases} H-\frac{f^2(L-x)^2}{2g'}, & x\leqslant L,\\ H, & x>L,\end{cases} \tag{18}$$

where, as mentioned, L is the width of the current.

From (18) it follows that, along the wall ($x=0$),

$$h(0,y)=H-\frac{f^2L^2}{2g'},\quad y<0. \tag{19}$$

Since the transport of the geostrophic boundary current through the zonal segment AB (Fig. 4) must be the same as the transport of the separated geostrophic current through the meridional segment BC (Fig. 4), we have,

$$\frac{g'}{2f}\left[H^2-h^2(0,y_\mathrm{s})\right]=\frac{g'}{2f_0}H^2,$$

implying that,

$$h(0,y)=H\left(\frac{\beta|y|}{f_0}\right)^{1/2},\quad y<0, \tag{20}$$

where f_0 is the Coriolis parameter at $y=0$. Note that the upper layer thickness h in (20) vanishes at $y=0$, so that the separation condition is satisfied. The actual separation latitude may be a Rossby radius distance away from $y=0$, because the geostrophic assumption is not valid in the vicinity of the separation point.

Since $|y_s| \sim O(R_{de})$, it follows that $\beta|y_s|/f_0 \sim O(\varepsilon^{5/6})$, implying that, to leading order,

$$L = 2^{1/2} R_d. \tag{21}$$

By combining (17), (18), and (21), we find that the momentum flux imparted on the region S by the upstream boundary current through the zonal segment AB (Fig. 4) is (to leading order)

$$\int_0^L hv^2 \, dx = \frac{1}{15} 2^{5/2} f_0^2 H R_d^3. \tag{22}$$

This relationship, which merely represents the value of the momentum flux for a zero PV boundary current, will be employed shortly.

2.3.2. Zero-pv eddy

The right-hand side of (16) includes contributions from both the eddy and the separated current surrounding it. It can be shown that the second contribution can be scaled as $O(\beta R_d R_{de} g' H^2/f_0)$ and that its ratio to the term $\beta \iint_{\text{eddy}} \psi \, dx \, dy$ is of $O(\varepsilon^{5/6})$. So, to find an estimate for the β term we can take $\psi = \psi_e$, where ψ_e is the zero-pv eddy streamfunction.

For a zero-pv eddy,

$$v_\theta = \frac{-f_0 r}{2}, \quad r \leqslant R \tag{23}$$

$$h_e = H_e \left(1 - \frac{r^2}{R_1^2}\right), \quad r \leqslant R, \tag{24}$$

where v_θ is the orbital speed, r is the radial distance from the center of the eddy, h_e is the eddy upper layer thickness, H_e is the maximum eddy thickness, and $R_1 = (8 g' H_e)^{1/2}/f_0$. It follows from (24) that the eddy radius is

$$R = \left[\frac{8 g'(H_e - H_b)}{f_0^2}\right]^{1/2}, \tag{25}$$

where H_b is the depth on the closed streamline bounding the eddy. The corresponding streamfunction for the eddy is

$$\psi_e = \frac{f_0^3}{2^6 g'} \left(R_1^2 - r^2\right)^2 - \frac{g' H_b^2}{2 f_0}, \quad r \leqslant R, \tag{26}$$

where the condition $\psi_e = g' H_b^2/2 f_0$ at $r=R$ has been used. Note that, as should be the case, this solution does not only conserve the pv along the streamlines, but also conserves the Bernoulli function. This is so because the eddy's streamlines are closed so that the Bernoulli function inside the eddy ($g' H_e$) need not be equal to that outside the eddy ($g' H$).

As a consequence of (14), we have $H_e \sim O(\varepsilon^{-2/6} H)$, and in view of (25) and (26) it follows that, to the leading order, $R = R_1$ and the streamfunction is

$$\psi_e = \frac{f_0^3}{2^6 g'} \left(R^2 - r^2\right)^2, \quad r \leqslant R, \tag{27}$$

which can be integrated over the eddy to give,

$$\iint_{\text{eddy}} \psi_e \, dx \, dy = 2^{-6} \left(\frac{\pi}{3}\right) \frac{f_0^3}{g'} R^6. \tag{28}$$

Like (22), (28) will be shortly used to obtain our solution.

2.3.3. Final solution

By substituting (22) and (28) into (16), we obtain our desired nonlinear eddy scale,

$$R = 2 \left(\frac{2^{5/2}}{5\pi}\right)^{1/6} \frac{R_d}{\varepsilon^{1/6}} \tag{29}$$

Relation (29) is an analytical estimate for the eddy radius based on our momentum balance approach. It relates the eddy size to the known physical parameters upstream and shows that the eddy is quite larger than its parent WBC ($R \approx 2 R_d/\varepsilon^{1/6}$). Note that (29) is a lower-bound estimate for the eddy radius, because the zero-pv eddy is highly nonlinear and, hence, is the steepest anticyclonic eddy possible.

As is frequently the case (see e.g., Nof and Pichevin, 1999), the radius of the eddy goes to infinity as $\beta \to 0$. This is not an issue and is merely a reflection of the expansion's character. That is to say, our expansion is a singular perturbation expansion rather than a regular expansion, implying that it is meaningful near the limit $\beta = 0$ but not at the limit itself. While this may appear peculiar, it is a common trait of perturbation expansions (see e.g., Bender and Orszag, 1999). Physically, this

singularity is due to the lack of a steady solution for an inviscid WBC separation on an f plane.

3. Numerical simulations

We have performed numerical simulations to test our analytical result and further investigate the role of β in the eddy formation. In these simulations, we compared the evolution of the system on both the f plane and the β plane (for the same set of physical parameters).

3.1. Numerical model description

We used a reduced gravity version of the isopycnic model developed by Bleck and Boudra (1981, 1986) and later improved by Bleck and Smith (1990). This model is suitable for our study since it allows isopycnic outcropping by using the "Flux-Corrected Transport" algorithm (Boris and Book, 1973; Zalesak, 1979) in the continuity equation.

The equations of motion are the two momentum equations,

$$\frac{\partial u}{\partial t}+u\frac{\partial u}{\partial x}+v\frac{\partial u}{\partial y}-(f_0+\beta y)v=-g'\frac{\partial h}{\partial y}+\frac{v}{h}\nabla\bullet(h\nabla u),$$

$$\frac{\partial v}{\partial t}+u\frac{\partial v}{\partial x}+v\frac{\partial v}{\partial y}-(f_0+\beta y)u=-g'\frac{\partial h}{\partial y}+\frac{v}{h}\nabla\bullet(h\nabla v),$$

and the continuity equation,

$$\frac{\partial h}{\partial t}+\frac{\partial(hu)}{\partial x}+\frac{\partial(hv)}{\partial y}=0,$$

where v is the frictional coefficient.

The model uses the Arakawa (1966) C-grid where the u-velocity points are shifted one-half grid step to the left from the h points, the v-velocity points are shifted one-half grid step down from the h points, and the vorticity points are shifted one-half grid step down from the u-velocity points. The integration domain is a rectangle with closed western and northern boundaries, open eastern boundary, and imposed inflow on the southern boundary. The Orlanski (1976) second-order radiation boundary condition was implemented on the open boundary.

Three extensive experiments were performed and the respective parameters are listed in Table 1. Additional experiments are not necessary for two reasons. First, the parameter controlling the experiment is the undisturbed upper layer thickness H as it sets up both the boundary current transport ($g'H/2f_0$) and the Rossby deformation radius R_d. Therefore, all the boundary current parameters are determined by H, and consequently, after nondimensionalizing, the equations of motion of any two runs would differ only by the nondimensional ($\beta R_d/f_0$) and the nondimensional frictional coefficient ($v/f_0R_d^2$) As long as the WBC is inertial, the parameter $\beta R_d/f_0$ is the only one that is controlling the experiment. Furthermore, in midlatitude the parameter $\beta R_d/f_0$ does not vary much and, consequently, the three experiments are sufficient. Second, for each of the three experiments that are conducted, we let the model run for 10,000 days, giving a massive data set.

The parameters adopted for the main experiment E1 are given in Table 1. The baroclinic Rossby deformation radius is 25 km and the transport of the boundary current is about 7.7 Sv ($1\,\mathrm{Sv}=10^6\,\mathrm{m^3\,s^{-1}}$). For economical reasons, we

Table 1
List of experiments

Experiment	Parameters	Resolution time step	Basin size
E1	$f_0=0.8573\times10^{-4}\,\mathrm{s^{-1}}$, $\beta=849\times10^{-11}\,\mathrm{m^{-1}\,s^{-1}}$, $g'=0.014\,\mathrm{m\,s^{-2}}$, $H=300\,\mathrm{m}$, $v=1500\,\mathrm{m^2\,s^{-1}}$	15 km, 12 min	1500 km × 3000 km
E2	$f_0=0.8573\times10^{-4}\,\mathrm{s^{-1}}$, $\beta=1.849\,10^{-11}\,\mathrm{m^{-1}\,s^{-1}}$, $g'=0.014\,\mathrm{m\,s^{-2}}$, $H=300\,\mathrm{m}$, $v=500\,\mathrm{m^2\,s^{-1}}$	15 km, 12 min	1500 km × 3000 km
E3	$f_0=0.8573\times10^{-4}\,\mathrm{s^{-1}}$, $\beta=0$, $g'=0.014\,\mathrm{m\,s^{-2}}$, $H=300\,\mathrm{m}$, $v=500\,\mathrm{m^2\,s^{-1}}$	15 km, 12 min	1500 km × 3000 km

took a time step of 720 s and a grid size of 15 km, so that we were barely resolving the Rossby radius. Since the eddy is much greater than the Rossby radius, this is not an issue, but it might be an issue for the WBC resolution. It would, of course, have been better to use a higher resolution. However, as we shall see, the results are so robust that this apparent weakness is probably not significant. We adopted the free slip boundary condition and a relatively large horizontal friction ($v = 1500\,m^2\,s^{-1}$) in order to smooth out transient features. We examined lower values of and found no significant differences. Also, our plots of the various terms in the equations (shown later) illustrate that, even though our chosen v is relatively high, its effect is negligible.

The above is true for both the f plane and the β plane runs. On an f plane, an increased viscosity caused an increase in both the separated and unseparated current width because the width of the currents is controlled by friction. On a β plane, on the other hand, the WBC width is controlled by inertia rather than friction and, consequently, an increased viscosity merely causes an increase of the *downstream* width. The initial condition for the β plane experiments is the day 200 fields of an f plane run with a zonal "wall" dividing the domain. On the southern edge we used the same parameters as above, and on the northern edge the upper layer thickness is zero. We then took the "wall" out and, at the same time, turn β on. We then let the system evolve for 10,000 days.

For economical reasons, the parameters used in the numerical experiment E1 are not identical to those of the JES, where the EKWC has a transport of merely 1.5 Sv. For the real JES, the Rossby deformation radius would be smaller than what we chose and we would have to decrease the integration time step, making our runs more time consuming. This is not an issue (even though our β effect is stronger than that in the JES) because it merely makes our runs spin up faster.

3.2. General results

Figs. 5 and 7(b),(d) show the contour plots of the nondimensional upper layer thickness for the f plane run (experiment E3 in Table 1) at days 100, 500, 1000, and 3000. Recall that, according to the analytics, there cannot be a steady state on an f plane because, without β, there is no force that can balance the upstream momentum flux. To examine this predicted property, we let the f plane runs go for a long period of time (3000 days). We see that indeed there is no steady state and, furthermore, there is no eddy. The most important aspect is that there is no eddy. Even though there is an area of increased upper layer thickness and transport due to an accumulation of fluid displaced from the western boundary, the resulting circulation is much weaker than that of the β plane run (Fig. 7(a),(c)). It can be seen that the entire system moves offshore and, consequently, it cannot reach a steady state. In order to highlight the offshore movement of the system, we plotted in Fig. 6 the 0.3 contour for each of the days depicted in Fig. 5. In analogy with the ballooning outflow situation studied by Nof and Pichevin (2001), the eastward movement of the separated boundary current produces a Coriolis force directed to the south

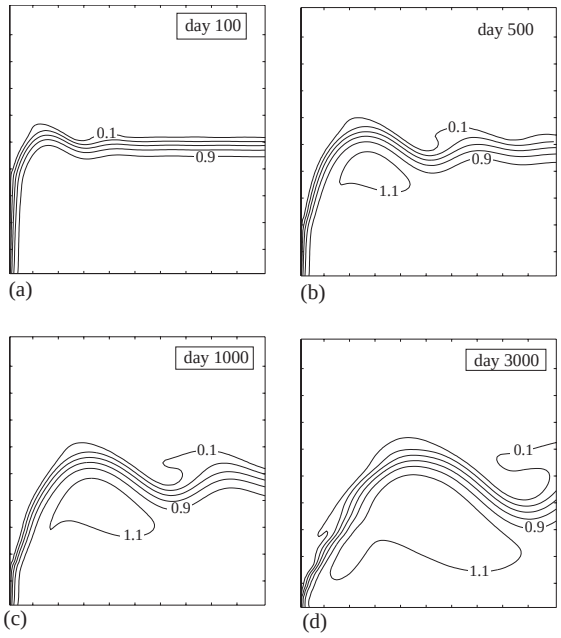

Fig. 5. ($a-d$) Contour maps of the upper layer thickness nondimensionalized by H = 300 m for the f plane run (experiment E3 in Table 1) at days 100, 500, 1000, and 3000. The contour spacing is 0.2. The axis marks are 10 grid points (150 km) apart.

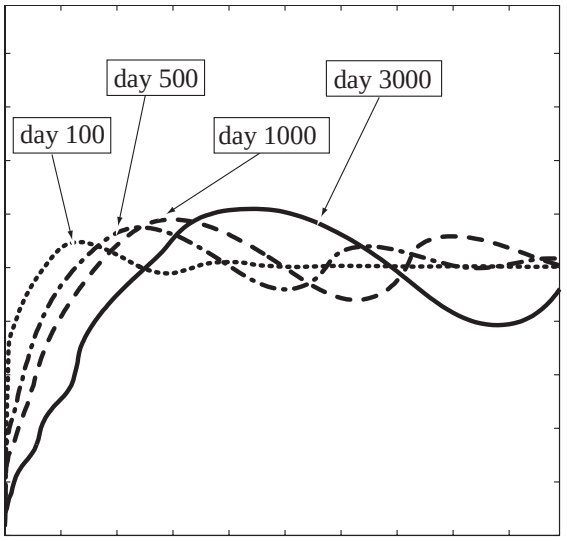

Fig. 6. Superposition of the 0.3 contours for the f plane run (experiment E3 in Table 1) at day 100, 500, 1000, and 3000, showing the offshore movement of the system.

(i.e., to the right of the direction of migration). This force balances the northward momentum flux (i.e., flow force) of the upstream northward flowing separated boundary current.

In Fig. 7, we plotted (side by side) snapshots of the (nondimensional) upper layer thickness and (nondimensional) streamfunction at day 3000 for the β plane experiment E1 and f plane experiment E3 (Table 1). This day is chosen as representative of the entire experiment E1 because it reflects the final steady solution. Note that, because the inflow and outflow mass fluxes are kept constant, there is virtually no variability after the decay of the initial oscillations generated during the spin-up. We see (from Figs. 7(a),(c)) that the intrusion eddy is a very prominent feature of the β plane plots with a maximum (nondimensional) upper layer thickness greater than 1.3 and a maximum (nondimensional) transport of 2. It is important to note that the boundary current is inertial (i.e., nonlinear) as its width is $O(R_d) = 25$ km, much smaller than the frictional boundary layer width $O(v/\beta)^{1/3} = 200$ km. Here, the friction used is high enough to avoid the transient features but not so large as to change the dynamics of the boundary current. The downstream zonal flow is broad compared with the upstream boundary current due to frictional

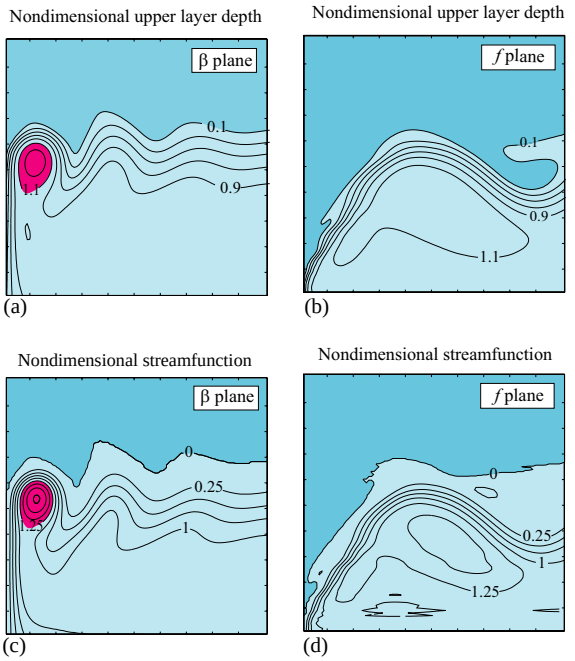

Fig. 7. Snapshots at day 3000. (a) Contour map of the nondimensional upper layer thickness (h/H) for the β plane run (experiment E1 in Table 1). Contour spacing of 0.2; (b) same as in (a) for the f plane run (experiment E3 in Table 1); (c) contour map of the nondimensional streamfunction ($\psi/(g'H/2f_0)$) for the β plane run (experiment E1 in Table 1). Contour spacing of 0.25; (d) same as in (c) for the f plane run (experiment E3 in Table 1). The axis marks are 10 grid points (150 km) apart.

diffusivity. To go further with the comparison of the numerical results to our analytical relations, we use (8) and rewrite (7) as

$$\underbrace{\int_0^L hv^2\,\mathrm{d}x}_{\textit{momentum flux}} + \underbrace{\frac{g'}{2}h^2(0,y_s)L_2}_{\textit{pressure}} - \underbrace{\beta\iint_S \psi\,\mathrm{d}x\,\mathrm{d}y}_{\beta-\text{force}} = 0, \tag{30}$$

where L is the boundary current width and L_2 is the length of the segment AB (see Fig. 4) and we took $\psi = 0$ on the wall. In this form, (30) represents a balance between three forces. The first is the northward force associated with the momentum flux of the alongshore current. The second is the northward pressure force due to the difference in thickness (on the wall) between points A and D (Fig. 4). The third term is the southward β force

resulting from the fact that a particle circulating anticyclonically within the eddy senses a larger Coriolis force on the northern side than it senses on the southern side of the path.

Fig. 8 displays the first term and the difference between the third and second terms (30). It is evident that the intrusion eddy exists in order to balance the northward momentum flux of the WBC because, according to (16) and the scale analysis, the eddy is the major contributor for the net β term (i.e., the combination of the second and third terms in (30)).

As stated before, the frictional coefficient used acts merely to smooth out transient features and does not play an important role in the integrated momentum balance. This can be seen from Figs. 8 and 9, which show that there are no significant frictional forces. To further verify that this is indeed the case, we performed experiment E2 (Table 1) with lower friction and we achieved essentially the same results as in E1. The only difference between the two is that, here, the separated current showed meanders that eventually closed upon themselves, pinching off small eddies (compared to our relatively large intrusion eddies) that died off (or were reattached to the main flow after some time).

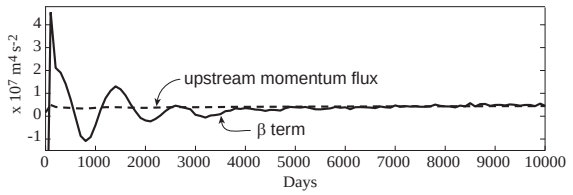

Fig. 8. Estimate of the terms in Eq. (30) from experiment E1 (Table 1). Dashed line: $\int_0^L hv^2$; solid line: $\beta \iint_S (\psi - \psi_\infty)\,\mathrm{d}x\,\mathrm{d}y$.

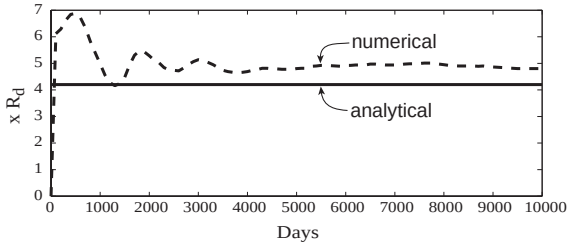

Fig. 9. Solid line: analytical estimate of the eddy radius from Eq. (30). Dashed line: Numerical estimate (adopting the value of 1.3 for the nondimensional bounding streamline of the eddy). Both radius estimates are scaled by the Rossby radius.

In Fig. 9 we show the analytical estimate of the eddy radius from (29) against the numerical estimate (taking the 1.3 closed (nondimensional) streamline as the eddy boundary (Fig. 7)). As expected, the radius based on the zero potential vorticity assumption is a lower bound for the actual eddy radius because, as mentioned, the zero-pv eddy is the steepest possible eddy. Nevertheless, the agreement is pretty good, as we get $4.2R_\mathrm{d}$ for the analytical estimate and about $5R_\mathrm{d}$ (after day 1000) for the numerical estimate.

4. The linear dynamics

We shall now show that for a small Rossby number flow (i.e., a linear geostrophic flow) there is no eddy associated with the current separation from the coast. In the linear limit, the boundary current width is large (due to the frictional nature of the boundary layer) compared with the Rossby radius so that the current is slower and the associated momentum flux is negligible. As we will see, in this situation, the frictional dissipation balances the β term in the boundary layer and no eddy is necessary.

Consider the familiar, steady linear reduced-gravity (depth integrated) equations of motion for the upper layer,

$$-fvh = -\frac{g'}{2}\frac{\partial(h^2)}{\partial x} + \frac{\tau^x}{\rho}, \tag{31}$$

$$fuh = -\frac{g'}{2}\frac{\partial(h^2)}{\partial y} - \kappa vh, \tag{32}$$

$$\frac{\partial(uh)}{\partial x} + \frac{\partial(vh)}{\partial y} = 0, \tag{33}$$

where κ is the interfacial friction coefficient. In the inviscid interior, Sverdrup dynamics dominates the field. Within the WBC, interfacial friction dissipates the energy input of the wind over the entire basin.

4.1. Momentum balance in the whole domain

Integrating the y-momentum equation (32) over the entire shaded area S (containing the WBC) bounded by $ABCD$ in Fig. 10, and assuming that $\psi=0$ on the bounds of the region containing the upper layer, we find,

$$\int_0^{x_B}\left[\frac{g'}{2}h^2-(f_0+\beta y)\psi\right]\mathrm{d}x-\beta\iint_S\psi\,\mathrm{d}x\,\mathrm{d}y$$

$$-\kappa\int_{y_s}^{y_n}\psi|_{x=L}\mathrm{d}y=0, \tag{34}$$

where L is the boundary current width, $\psi|_{x=L}$ is the streamfunction at $x=L$, x_B is the x-component of B, and y_s and y_n are the y-components of A and D, respectively (Fig. 10). We shall now leave (34) aside for moment and discuss the interior.

4.2. The interior balance

We note from (32) that, in the inviscid ocean interior (where friction is unimportant),

$$\frac{\partial}{\partial y}\left[\frac{g'}{2}h^2-(f_0+\beta y)\psi\right]=-\beta\psi, \tag{35}$$

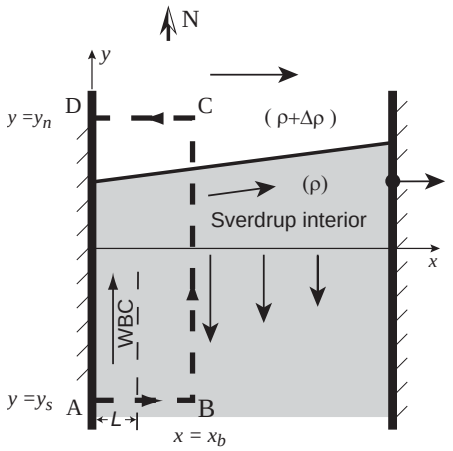

Fig. 10. Schematic diagram of the separation in the hypothetical linear limit, i.e., the boundary current is taken to be a linear frictional current rather than inertial. The circulation is established by both the wind and the throughflow induced by the outflow. In the basin interior the slow southward Sverdrup flow takes place, while in the narrower WBC (of width L) a stronger northward WBC closes the anticyclonic gyre. In this linear limit, the boundary current leaves the coast by vanishing the upper layer thickens in Eq. (31) (á là Parsons, 1969).

which can be integrated from y_s to y_n to give

$$\left[\frac{g'}{2}h^2-(f_0+\beta y)\psi\right]_{y=y_s}=\beta\int_{y_s}^{y_n}\psi\mathrm{d}y, \tag{36}$$

for any $x>L$. Integrating (36) from $x=L$ to $x=x_B$, we get,

$$\int_L^{x_B}\left[\frac{g'}{2}h^2-(f_0+\beta y)\psi\right]dx-\beta\int_L^{x_B}\int_{y_s}^{y_s}\psi\,\mathrm{d}y\,\mathrm{d}x=0, \tag{37}$$

This balance is valid in the integration domain (S) within the ocean interior (shown in Fig. 10).

4.3. The western boundary layer balance

Subtracting (37), which governs the interior, from (34), which governs the entire region (WBC plus interior), we obtain for the WBC ($0\leqslant x\leqslant L$),

$$\int_0^{L}\left[\frac{g'}{2}h^2-(f_0+\beta y)\psi\right]\mathrm{d}x-\beta\int_{y_s}^{y_n}\int_0^{L}\psi\,\mathrm{d}x\,\mathrm{d}y$$

$$-\kappa\int_{y_s}^{y_n}\psi|_{x=L}\,\mathrm{d}y=0. \tag{38}$$

Neglecting the wind stress term within the boundary current, it follows from (31) that,

$$\frac{g'}{2}h^2-(f_0+\beta y)\psi=C,\ x\leqslant L \tag{39}$$

where $C=\beta\int_{y_s}^{y_n}\psi|_{x=L}\,\mathrm{d}y$ and a matching of (39) and (36) at $x=L$ has been invoked. Substituting (39) into (38), we obtain,

$$\beta\int_{y_s}^{y_n}\int_0^{L}(\psi-\psi|_{x=L})\,\mathrm{d}x\,\mathrm{d}y$$

$$+\kappa\int_{y_s}^{y_n}\psi|_{x=L}\,\mathrm{d}y=0. \tag{40}$$

The integrand of the second term of (40) is positive, implying that the first term should be negative. Note that, in this case, an anticyclonic eddy would make a negative contribution to the β term. By scaling (40), we see that the WBC *by itself* produces a β force that is able to balance the frictional dissipation terms. This is the case as long as $L\sim O(\kappa/\beta)$, which is the well-known Stommel boundary layer scale.

We see that (40) represents a balance between the β-force in the WBC and the frictional

dissipation of the integrated wind stress curl over the entire basin. Under these conditions, no eddy is necessary for the required momentum balance, showing that the establishment of the intrusion eddy is due to inertia (nonlinearities) and β.

5. Conclusions

Taking into account that the EKWC is forced to separate from the coast by an outflow to the east and the upstream (northward) throughflow that it introduces, we derived a theory for the existence of the "intrusion eddy." Our analytical relations and numerical simulations show that, without the generation of the eddy, the nonlinear momentum flux of the northward-flowing boundary current on a β plane could not have been balanced. On an f plane, the situation is quite different. To balance the northward momentum force imparted by the boundary, the system simply moves offshore (Fig. 6), producing a southward Coriolis force.

On this basis, we argue that the existence of the UWE may not be related to instabilities but rather may be due to β and nonlinearities (Figs. 7 and 8). (A similar no-instability argument related to the African coastline curvature was put forward by Ou and de Ruijter (1986) as an explanation for the Agulhas Current retroflection.) Further, we argue that the UWE semi-permanent characteristic may not be due to topographic arrest, but rather is part of the dynamics, which includes the generation of permanent eddy (Fig. 7(a),(c)). Although our analysis strongly suggests that this is the case, we could not prove either the topography or the stability issue. This is because our reduced gravity model does not contain mixed barotropic/baroclinic instabilities, nor does it contain bottom topography (see e.g., Hogan and Hurlburt, 2000). For a mean transport of $\sim$1.5 Sv for the EKWC, we find a Rossby radius of 16.3 km and an $\varepsilon^{1/6}$ of 0.39. Our predicted value for the UWE diameter (from (30)) is then 141 km, which agrees fairly well with the observed 150 km radius (Fig. 2), suggesting that its generation is related to the mechanism proposed here.

This generation process is only relevant when EKWC is strong and, hence, nonlinear (Mitchell, 2003). In times where the EKWC is weak and linear, there is no eddy formation, in agreement with the observations. It is important to realize here that our steady solutions merely imply that the period during which the current is strong (or weak) is longer than $(\beta R_d)^{-1}$, a condition which is obviously satisfied.

The present theory is not applicable to the Gulf Stream and Brazil-Malvinas confluence for three reasons. First, in both cases, there are strong opposing (cold) currents (the Labrador current in the first case and the Malvinas current in the second) whose momentum fluxes cannot be neglected (see e.g., Arruda and Nof, 2003). Second, there is a marked difference in density between the two colliding currents so that the denser (colder) current would slide under the less dense current and even separate from the coast in different latitude. Third, there is a coastline tilt in both cases that could cause significant change in the momentum balance.

Acknowledgements

This study was supported by National Science Foundation grants OCE 9911324 and OCE 0241036; National Aeronautics and Space Administration grants NAG5-7630 and NAG5-10860; and Office of Naval Research grant N00014-01-0291. Wilton Z. Arruda was funded by Conselho Nacional de Desenvolvimento Científico e Tecnológico (CNPq-Brazil) under grant 202436/91-8 and a fellowship from the Inter-American Institute for Global Change Research (IAI) through the South Atlantic Climate Change Consortium (SACC). COAPS receives its base support from a Secretary of the Navy grant to James J. O'Brien. The authors would like to thank Dr. Nabuo Suginohara and Dr. Steven Ramp for their helpful comments and careful reading of the manuscript.

References

Agra, C., Nof, D., 1993. Collision and separation of boundary currents. Deep-Sea Research I 40, 2259–2282.

Arakawa, A., 1966. Computational design for long-term numerical integration of the equations of fluid motion.

Two dimensional incompressible flow. Part I. Journal of Computational Physics 1, 119–143.

Arruda, W., Nof, D., 2003. The Mindanao and Halmahera eddies are due to the bending of their parent currents, β and nonlinearities. Journal of Physical Oceanography 33, 2815–2830.

Bender, C.M., Orszag, S.A., 1999. Advanced Mathematical Methods for Scientists and Engineers: Asymptotic. Springer, Berlin 593pp.

Bleck, R., Boudra, D., 1981. Initial testing of a numerical ocean circulation model using a hybrid, quasi-isopycnic vertical coordinate. Journal of Physical Oceanography 11, 755–770.

Bleck, R., Boudra, D., 1986. Wind-driven spin-up in eddy-resolving ocean models formulated in isopycnic and isobaric coordinates. Journal of Geophysical Research 91, 7611–7621.

Bleck, R., Smith, L.T., 1990. A wind-driven isopycnic coordinate model of the North and Equatorial Atlantic Ocean, 1, Model development and supporting experiments. Journal of Geophysical Research 95, 3273–3285.

Boris, J.P., Book, D.L., 1973. Flux-corrected transport. I. SHASTA, a fluid transport algorithm that works. Journal of Computational Physics 11, 38–69.

Cho, Y.-K., Kim, K., 1996. Seasonal variation of the East Korea Warm Current and its relation with the cold. water. La Mer 34, 172–182.

Chu, P.C., Lan, J., Fan, C.W., 2001. Japan Sea circulation and thermohaline structure, Part 1, Climatology. Journal of Physical Oceanography 31, 244–271.

Dengg, J., Beckmann, A., Gerdes, R., 1996. The Gulf Stream Separation Problem. In: Krauss, W. (Ed.), Warm waters phere of North Atlantic Ocean. Gebr. Bornträger, Sttutgard, pp. 253–290.

Gordon, A.L., 1990. Sea of Japan. In: Marginal Seas and the Kuroshio: An Assessment of Mutual Impact. Department of Oceanography, Florida State University, Tallahassee, FL, USA.

Gordon, A.L., Giulivi, C.F., Lee, C.M., Furey, H.H., Bower, A., Talley, L., 2002. Japan/East Sea intrathermocline eddies. Journal of Physical Oceanography 32, 1960–1974.

Hogan, P.J., Hurlburt, H., 2000. Impact of upper ocean-topographical coupling and isopycnal outcropping in Japan/East Sea models with 1/8 to 1/64 resolution. Journal of Physical Oceanography 30, 2535–2561.

Holloway, G., Sou, T., Eby, M., 1995. Dynamics of circulation of the Japan Sea. Journal of Marine Research 53, 539–569.

Huang, R.X., Flierl, G.R., 1987. Two-layer models for the thermocline and current structure in subtropical/subpolar gyres. Journal of Physical Oceanography 17, 872–884.

Ichiye, T., Takano, K., 1988. Mesoscale eddies in the Sea of Japan. La Mer 26, 69–79.

Isoda, Y., Nishihara, M., 1992. Behavior of warm eddies in the Japan Sea. Umi to Sora 67 (Spec. Issue), 231–243.

Isoda, Y., Saitoh, S.-I., 1993. The northward intruding eddy along the coast of Korea. Journal of Oceanography 49, 443–458.

Jacobs, G.A., Perkins, H.T., Teague, W.J., Hogan, P.J., 2001. Summer transport through the Tsushima-Korea Strait. Journal of Geophysical Research 106, 6917–6929.

Kang, H.E., Kang, Y.Q., 1990. Spatio-temporal characteristics of the Ulleung Warm Lens. Bulletin of the Korean Fisheries Society 203, 407–415.

Katoh, O., 1994. Structure of the Tsushima Current in the southwestern Japan Sea. Journal of Oceanography 50, 317–338.

Kawabe, M., 1982a. Branching of Tsushima Current in the Japan Sea. Part I. Data Analysis. Journal of the Oceanographical Society of Japan 38, 95–107.

Kawabe, M., 1982b. Branching of Tsushima Current in the Japan Sea. Part II. Numerical experiment. Journal of the Oceanographical Society of Japan 38, 183–192.

Killworth, P.D., 1983. On the motion of isolated lenses on a beta-plane. Journal of Physical Oceanography 13, 368–376.

Kim, C.H., Kim, K., 1983. Characteristics and origin of the cold water mass along the east coast of Korea. Journal of the Oceanological Society of Korea 18, 73–83.

Kim, K., Legeckis, R., 1986. Branching of the Tsushima Current in 1981–83. Progress in Oceanography 17, 265–276.

Kim, K., Kim, K.-R., Chung, J., Yoo, H., Park, S., 1991. Characteristics of physical properties in the Ulleung Basin. Journal of the Oceanological Society of Korea 26, 83–100.

Lebedev, I., Nof, D., 1996. The drifting confluence zone. Journal of Oceanography 26, 2429–2448.

Lebedev, I., Nof, D., 1997. Collision of boundary currents: beyond a steady state. Deep-Sea Research I 44, 771–791.

Lie, H.-J., 1984. Coastal current and its variation along the east coast of Korea. In: Ichiye, T. (Ed.), Ocean Hydrodynamics of the Japan and East China Seas. Elsevier, Amsterdam, pp. 399–408.

Lie, H.-J., Byun, S.-K., 1985. Summertime southward current along the east coast of Korea. Journal of the Oceanological Society of Korea 20, 22–27.

Lie, H.-J., Byun, S.-K., Bang, I., Cho, C.-H., 1995. Physical structure of eddies in the southwestern East Sea. Journal of the Korean Society of Oceanography 30, 170–183.

Lim, B., Kim, K., 1995. A numerical study on the interaction of the Ulleung Warm Eddy with topography and lateral boundary. Journal of the Oceanological Society of Korea 30, 565–583.

Matsuyama, M., Kurita, Y., Senjyu, T., Koike, Y., Hayashi, T., 1990. The warm eddy observed east of Oki Islands in the Japan Sea (2). Umi to Sora 66, 67–75.

Mitchell, D.A., 2003. Upper current structure and variability in the southwestern Japan/East Sea. Ph.D. Dissertation, University of Rhode Island, Providence, RI, 159pp.

Miyao, T., 1994. The fractal dimension analysis applied to eddies in the Sea of Japan. Oceanographical Magazine 44, 13–30.

Nilsson, C.S., Cresswell, G.R., 1980. The formation and evolution of East Australia Current warm-core eddies. Progress in Oceanography 9, 133–183.

Nof, D., 1981. On the dynamics of equatorial outflows with application to the Amazon basin. Journal of Marine Research 39, 1–29.

Nof, D., 2003. The Southern Ocean's grip on the northward meridional flow. Progress in Oceanography 56, 223–247.

Nof, D., Pichevin, T., 1999. The establishment of the Tsugaru and the Alboran gyres. Journal of Physical Oceanography 29, 39–54.

Nof, D., Pichevin, T., 2001. The ballooning of outflows. Journal of Physical Oceanography 31, 3045–3058.

Olson, D.B., 1991. Rings in the ocean. Annual Review of Earth and Planetary Sciences 19, 283–311.

Orlanski, I., 1976. A simple boundary condition for unbounded hyperbolic flows. Journal of Computational Physics 21, 251–269.

Ou, H.W., 2001. A model of buoyant throughflow with application to branching of the Tsushima Current. Journal of Physical Oceanography 31, 115–126.

Ou, H.W., Gordon, A.L., 2002. Subduction along a midocean front and the generation of intra-thermocline eddies: a theoretical study. Journal of Physical Oceanography 32, 1975–1986.

Ou, H.W., de Ruijter, W.P.M., 1986. Separation of an inertial boundary current from a curved coastline. Journal of Physical Oceanography 16, 280–289.

Parsons, A.T., 1969. A two-layer model for Gulf Stream separation. Journal of Fluid Mechanics 39, 511–528.

Perkins, H., Teague, W.J., Jacobs, G.A., Change, K.I., Suk, M.-S., 2000. Currents in Korea–Tsushima Strait during summer 1999. Geophysical Research Letters 27, 3033–3036.

Preller, R., Hogan, P., 1998. Oceanography of the Sea of Okhotsk and the Japan/East Sea coastal segment. In: Robinson, A., Brink, K. (Eds.), The Sea, 11. Wiley, New York, pp. 429–481.

Ramp, S.R., Bahr, F.L., Ashjian, C.J., Talley, L.D., 2003. The Upper-Ocean Circulation in the Ulleung Basin during June–July 1999. Deep-Sea Research II, submitted.

Rostov, I., Yurasov, G.I., Rudyh, N.I., Moroz, V.V., Dmitrev, E.V., Nabiullin, A.A., Khrapchenkov, F.F., Bunim, V.M., 2001. Oceanographic Atlas of the Bering Sea, Okhotsk Sea, and Japan/East Sea. CD-ROM, POI FEBRAS, Vladivostok, Russia.

Seung, Y-H., Kim, K., 1989. On the possible role of local thermal forcing on the Japan Sea Circulation. Journal of the Oceanological Society of Korea 24, 29–38.

Suda, K., Hidaka, K., 1932. The results of the oceanographical observations on board R.M.S. Syunpu Maru in the southern part of the Sea of Japan in the summer of 1929, Part I. Journal of the Oceanographical Imperial Marine Observatory 3, 291–375 (in Japanese).

Sugimoto, T., Tameishi, H., 1992. Warm-core rings, streamers and their role on the fishing ground formation around Japan. Deep-Sea Research I 39 (Suppl. S), S183–S201.

Tameishi, H., 1987. Applications of NOAA/AVHRR images to fisheries around Tsushima Strait. Fisheries Oceanography 51, 238–244.

Tanioka, K., 1968. On the East Korean Warm Current (Tosen Warm Current). Oceanographical Magazine 20, 31–38.

Toba, T., Tomizaqa, K., Kurasaw, Y., Hanawa, K., 1982. Seasonal and year to year variability of the Tsushima-Tsugaru Currents system with its possible cause. La Mer 20, 41–51.

Tomczak, M., Godfrey, J.S., 1994. Regional Oceanography: An Introduction. Pergamon Press, Oxford 422pp.

Uda, M., 1934. The results of simultaneous oceanographical investigations in the Japan Sea and its adjacent waters in May and June 1932. Journal of the Imperial Fisheries Experimental Station 5, 57–190 (in Japanese).

Veronis, G., 1973. Model of world ocean circulation: I. Wind driven, two-layer. Journal of Marine Research 31, 228–288.

Yoon, J.-H., Kawamura, H., 2002. The formation and circulation of the intermediate water in the Japan Sea. Journal of Oceanography 58, 197–211.

Zalesak, S.T., 1979. Fully multidimensional flux-corrected transport algorithms for fluids. Journal of Computational Physics 31, 335–362.